THE ROYAL SOCIETY

# Polymer combustion: effects of flame emissivity

By M. I. Nelson[1] and J. Brindley[2]

[1]*Fuel and Energy Department, and* [2]*Department of Applied Mathematics, University of Leeds, Leeds LS2 9JT, UK*

We present a nonlinear dynamical systems model developed to gain an insight into the flammability of polymeric materials. Regimes of particular interest from the viewpoint of fire retardancy are identified and exhibited in steady-state diagrams. The variation in parameter space of these regimes as a function of the emissivity of the flame is investigated.

**Keywords: cone calorimeter; flammability; polymers; radiative ignition; soot**

## 1. Introduction

The combustion of polymeric materials is a complicated process involving physical phenomena that are only partly understood. Complex chemical and physical processes occur in at least two phases: a solid phase, where pyrolysis occurs in response to an external heat source, and a gas phase where the pyrolysis products react further, usually to form a flame. There may also be a liquid phase.

Many of the physical and chemical processes that occur during polymer combustion are areas of research in their own right, e.g. gas-phase and pyrolysis kinetics, modelling the radiative heat-transfer from a flame, the fluid dynamics of flames, etc. In the most general setting the solid-phase problem involves solving a three-dimensional Stefan problem for the eroding boundary. Usually, one imagines that a material 'contracts' as it burns, but in the presence of fire retardants promoting intumescence the material may expand. Finally, the flammability of industrial products is further complicated because they are commonly composed of mixtures of materials having different chemical and physical properties.

Despite the complexity of these processes, significant insights into fire engineering problems have been gained by making appropriate approximations depending upon the subproblem being investigated (Drysdale 1987). One of the challenges for the future is to unify the various submodels in a rigorous manner.

Polymer flammability has no intrinsic meaning; the flammability of a polymer is defined by the test method used to measure it. In this paper we consider flammability within the context of the cone calorimeter (Babrauskas 1982, 1984; Babrauskas & Parker 1986), an experimental device that has provided a major step forward in the systematic investigation of ignition properties of polymeric materials. We consider the configuration when a material is heated from above by a radiative heater (figure 1*a*). For our purposes the essential feature of the test is that the sample receives a uniform flux from the heater across the exposed surface area.

*Phil. Trans. R. Soc. Lond.* A (1999) **357**, 3655–3673 

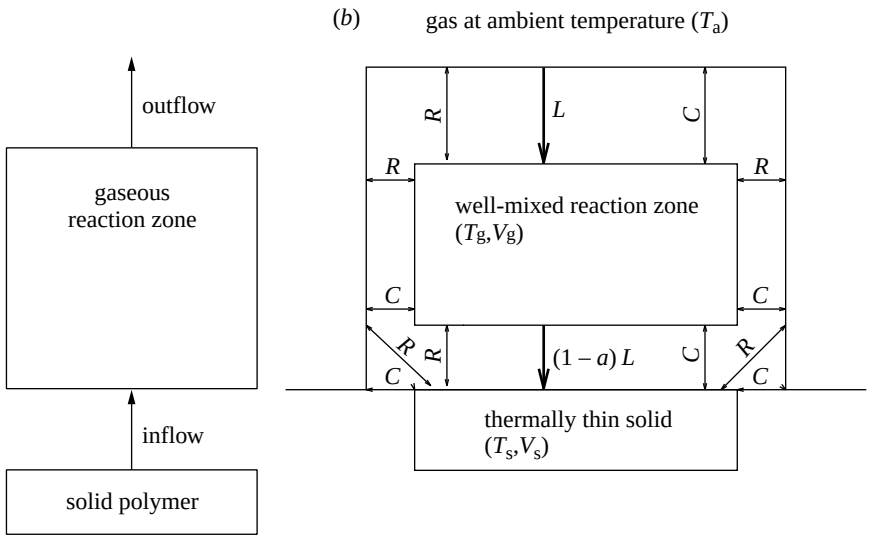


Figure 1. Schematic diagrams of the model geometry: (*a*) inflow/outflow; (*b*) heat-transfer processes modelled.

### (*a*) *Simplified models for polymer combustion*

As outlined above, a complete description of the mechanisms leading to the establishment of a flame over a burning surface requires consideration of mass and heat transport in both the gas and solid phases. The usual fire-engineering approach, when explicitly modelling the pyrolysis of polymers, is to ignore the complexities of gas-phase kinetics, defining ignition in terms of solid-phase properties. The most common approaches are to define criticality in terms of either a critical surface temperature, a *thermal pyrolysis model*, or a critical flowrate of volatiles into the gas-phase, a *critical mass flux model*. An overview of these approaches is presented elsewhere (Nelson 1998).

Although the overall phenomena are complicated, two salient processes, one in each phase, must occur if a material is to ignite. The solid must first decompose to release volatiles into the boundary layer. These gases must then mix with surrounding air to produce a flammable mixture, which then either autoignites or is ignited by an external source, such as a pilot flame. It has recently been demonstrated that these processes can be described by simple nonlinear dynamical systems models (Rychlý & Rychlá 1986, 1996; Búcsi & Rychlý 1992; Rychlý & Costa 1995; Nelson 1998).

An advantage of this approach is that ignition is no longer externally defined in terms of solid-phase properties, i.e. a critical surface temperature or a critical flowrate of volatiles. Instead ignition is intrinsic to the model: pyrolysis is an endothermic process, while combustion is exothermic, and the interaction between these processes determines ignition, as represented by an appropriate bifurcation.

Two models have been developed along these lines. In this paper we extend a model developed at Leeds for the radiative ignition of materials in the cone calorimeter. The Leeds group has investigated the steady-state structure of its model by a combination of direct integration and continuation methods (Nelson 1998).

An alternative model has been developed by Rychlý's research group (Rychlý &

Rychlá 1986, 1996; Búcsi & Rychlý 1992; Rychlý & Costa 1995). This is a more generic model, variations of which have been applied to the limiting oxygen index test (Búcsi & Rychlý 1992; Rychlý & Costa 1995) and the cone calorimeter (Rychlý & Costa 1995; Rychlý & Rychlá 1996). The Rychlý group has investigated its models using direct integration. There are several differences in approach between the models developed in Leeds and by Rychlý, and an area of current research in Leeds is to investigate the steady-state behaviour of the Rychlý models.

The specific feature we address in this paper is the effect of emissivity of the gas phase. This depends strongly upon the quantity of solid material in particulate form that is carried from the decomposing solid into the flame, and can be influenced by the chemical composition and physical properties of the polymer together with any additives that may be present. To a certain extent, therefore, the value of this emissivity may be 'designed' into the fabrication of the polymer as required by anti-flammability requirements.

## 2. Description of the model

As the assumptions underlying our model have been explained in detail elsewhere (Nelson 1998) we provide merely a conceptual overview.

The dynamics controlling the burning behaviour of a polymer are modelled by considering the interaction between three zones: the solid test material; the gaseous reaction zone (the 'flame'); and air at ambient temperature. For simplicity each zone is assumed to be well-mixed. The resulting model contains equations for solid phase and gas phase processes that are coupled through heat (convective and radiative) and mass transfer (figure 1). Thermoplastics soften when heated at defined temperatures and in some cases melt. Such processes are not included in this model. Our approach could be extended to cover these by considering physical and chemical processes in a molten 'melt zone' between the solid phase and the gas phase.

Polymer combustion chemistry is modelled by two first-order reactions obeying Arrhenius kinetics:

$$\mathcal{M}_1(\mathrm{s}) \rightarrow \mathcal{M}_2(\mathrm{g}), \tag{2.1}$$

$$\mathcal{M}_2(\mathrm{g}) + b_k \mathrm{O}_2(\mathrm{g}) \rightarrow (1 + b_k)\mathcal{M}_3(\mathrm{g}). \tag{2.2}$$

Reaction (2.1) represents the pyrolysis of the polymer ($\mathcal{M}_1$). The products of this reaction are gas-phase volatiles ($\mathcal{M}_2$), which flow in the gaseous reaction zone. These volatiles then undergo gas-phase oxidation, reaction (2.2). We assume that the concentration of oxygen in the flame is given by its concentration in the surrounding air, which is a good approximation for the standard conditions in which the cone calorimeter is used (Babrauskas 1984), so that our reaction scheme becomes two consecutive thermal degradation reactions.

The Arrhenius formulation for the pyrolysis kinetics is

$$k = -A_\mathrm{s} \exp\left[\frac{-E_\mathrm{s}}{RT_\mathrm{s}}\right]\mathcal{M}_1. \tag{2.3}$$

In investigating polymer combustion it has proven advantageous to use an alternative formulation (Nelson *et al*. 1995, 1996*a*, *b*, 1997; Nelson 1998) based upon the

concept of 'characteristic temperature'; writing

$$k = -\frac{\mathcal{H}E_\mathrm{s}}{RT_\mathrm{c}^2}\exp\left[\frac{E_\mathrm{s}}{R}\left(\frac{1}{T_\mathrm{c}}-\frac{1}{T_\mathrm{s}}\right)\right]\mathcal{M}_1, \tag{2.4}$$

where $T_\mathrm{c}$ is the 'characteristic temperature' measured in a thermogravimetric experiment (Hatakeyama & Quinn 1994) and $\mathcal{H}$ is an experimental parameter. Materials of practical interest have a characteristic temperature of at least 580 K and are usually in the range $580 \leqslant T_\mathrm{c}\,(\mathrm{K}) \leqslant 780$.

For a given 'material' we fix thermophysical properties and chemical properties and treat the heat flux from the ignition source, $\mathcal{L}$, the experimentally controlled parameter, as the primary bifurcation parameter. We are interested in questions such as the following:

1. What is the smallest value of the imposed irradiance that will ignite a material?

2. If a material is ignited and the irradiance subsequently decreased, is there a critical value of the irradiance at which the flame will extinguish itself?

3. What is the steady-state structure of the model and how does it correspond to flammability characteristics?

### (*a*) *Gas-phase emissivity*

The net emissivity of a flame depends upon the concentration of minute carbonaceous particles ('soot') within the flame and on the 'thickness', or mean beam length, of the flame. Various approximations are available in the literature to estimate the mean beam length and the soot concentration (Drysdale 1987).

For our purposes it suffices to note that the emissivity of non-luminous flames, such as methanol and paraformaldehyde, is very low, $\epsilon_\mathrm{g} \sim 0.07$, and that as the soot content increases the emissivity increases towards one; for thick luminous flames from hydrocarbon fuels, it is common to assume black-body behaviour, i.e. $\epsilon_\mathrm{g} = 1$. The flame emissivity can be affected by the addition of fire retardants. Therefore, rather than trying to calculate the emissivity for any particular material, we regard it as a free parameter.

There is no definition of the transition between non-luminous and luminous flames. For the purposes of this paper we define non-luminous flames as flames having an emissivity in the range $0 \leqslant \epsilon_\mathrm{g} \leqslant 0.1$ and luminous flames as flames having an emissivity of $0.1 < \epsilon_\mathrm{g} \leqslant 1.0$.

## 3. Model equations

The system that we study is (Nelson 1998)

$$\frac{\mathrm{d}\mathcal{M}_1}{\mathrm{d}t} = -R_p, \tag{3.1}$$

$$c_{p_s}\rho_s V_s\frac{\mathrm{d}T_s}{\mathrm{d}t} = Q_s R_p + \alpha_s(1-\alpha_g)S\mathcal{L} - S\chi_0(T_s - T_g) + \sigma([1-\mathcal{F}_{gs}]\alpha_s T_a^4 - \epsilon_s T_s^4)S + \alpha_s\mathcal{F}_{gs}\epsilon_g\sigma T_g^4 S, \tag{3.2}$$

$$\frac{\mathrm{d}\mathcal{M}_2}{\mathrm{d}t} = \frac{q_{\mathrm{inflow}}}{V_p} - \frac{q_{\mathrm{inflow}}\mathcal{M}_2}{V_g} - A_g\mathcal{M}_2\exp\left[\frac{-E_g}{RT_g}\right] - \frac{q_{\mathrm{reaction}}\mathcal{M}_2}{V_g}, \tag{3.3}$$

$$\frac{\mathrm{d}\mathcal{M}_3}{\mathrm{d}t} = A_g\mathcal{M}_2\exp\left[\frac{-E_g}{RT_g}\right] - q_{\mathrm{inflow}}\frac{\mathcal{M}_3}{V_g} - \frac{q_{\mathrm{reaction}}\mathcal{M}_3}{V_g}, \tag{3.4}$$

$$\begin{aligned} c_{p_g}\rho_g V_g\frac{\mathrm{d}T_g}{\mathrm{d}t} = {} & -Q_s R_p + Q_g A_g\mathcal{M}_2\exp\left[\frac{-E_g}{RT_g}\right] \\ & - S\chi_1(T_g - T_a) - S\chi_0(T_g - T_s) - 2\delta_g(x+y)\chi_1(T_g - T_a) \\ & + 2\sigma\epsilon_g\delta_1(x+y)(T_a^4 - T_g^4) + \sigma S(\alpha_g T_a^4 - \epsilon_g T_g^4) \\ & + \sigma S([1-\mathcal{F}_{sg}]\alpha_g T_a^4 - \epsilon_g T_g^4) + \alpha_g\epsilon_s\sigma\mathcal{F}_{sg}T_s^4 S + \alpha_g S\mathcal{L} \\ & - c_{p_g}\rho_g T_g q_{\mathrm{inflow}} - \frac{q_{\mathrm{reaction}}T_g}{V_g}, \end{aligned} \tag{3.5}$$

where

$$R_p = \frac{\mathcal{H}E_s}{RT_c^2}\exp\left[\frac{E_s}{R}\left(\frac{1}{T_c} - \frac{1}{T_s}\right)\right]\mathcal{M}_1, \tag{3.6}$$

$$V_p = \frac{RT_s}{\mathcal{W}_2\mathcal{P}^0}, \tag{3.7}$$

$$q_{\mathrm{inflow}} = R_p \cdot V_p, \tag{3.8}$$

$$q_{\mathrm{reaction}} = \left[\left(\frac{\mathcal{W}_2 - \mathcal{W}_3}{\mathcal{W}_2\mathcal{W}_3}\right)\cdot\frac{RA_g}{\mathcal{P}^0}\right]\exp\left[\frac{-E_g}{RT_g}\right]\mathcal{M}_2 T_g, \tag{3.9}$$

$$\mathcal{M}_1(0) = V_s\rho_s = S\delta_s\rho_s, \tag{3.10}$$

$$\mathcal{M}_2(0) = \mathcal{M}_3(0) = 0, \tag{3.11}$$

$$T_s(0) = T_g(0) = T_a. \tag{3.12}$$

See Appendix A for nomenclature. Note that equation (3.9) assumes that the gaseous reaction is thermal in nature, as discussed in § 2.

Equations (3.1)–(3.5) govern the behaviour of the test material in the pre-ignition region and, provided the sample ignites, through the post-ignition region until the flame is extinguished. As is usual in such problems we will investigate a steady-state problem, ignoring depletion of the test material (Drysdale 1987), the characteristic time for heat transfer in the solid being considerably shorter than that for mass change. Note that the products of the gas-phase reaction ($\mathcal{M}_3$) play no role in defining the dynamics of our system. Consequently, our model reduces to equations (3.2), (3.3) and (3.5).

For brevity we do not include the non-dimensionalized equations. The definitions of the non-dimensionalized temperature scale ($T_i^*$) and non-dimensionalized irradiance ($q_{\mathrm{ign}}$) are included in the appendix. It should be noted that the non-dimensionalized temperatures are defined with respect to ambient temperature, which is not a control variable in the cone calorimeter; the classic Frank–Kamenetskii variables are not used.

### (*a*) *Methodology*

We are concerned here with the sensitivity of the system to variations in the flame emissivity, $\epsilon_{\mathrm{g}}$, and the complexity of equations (3.2), (3.3) and (3.5) means that numerical methods are inevitable. Our approach is to characterize steady-state structures in terms of the burning behaviour exhibited by materials. Using dynamical systems methodology we show how regimes of practical interest are defined by the structure of the limit point bifurcation diagram.

For path following, AUTO94 (Doedel *et al*. 1994) was used. In the steady-state diagrams the standard representation is used: solid lines are stable steady states, dotted lines are unstable steady states, squares are Hopf bifurcation points, open circles are unstable periodic orbits and filled-in circles are stable periodic orbits. Homoclinic orbits are located by continuation of a limit cycle to large period (Doedel & Kernevez 1986). We are interested in the ignitability of our system, which corresponds experimentally to the establishment of a flame over the sample. Accordingly we principally investigate the variation of non-dimensionalized gaseous temperature ($T_{\mathrm{g}}^{*}$) with non-dimensionalized irradiance ($q_{\mathrm{ign}}$); when considering periodic solutions we plot the maximum value of $T_{\mathrm{g}}^{*}$ on the limit cycle.

In the steady-state diagrams, which represent the behaviour of a specific material, we use non-dimensionalized variables, while in the bifurcation diagrams, which represent the behaviour of a class of materials, and are therefore more important from a practical view, we use dimensionalized variables.

We refer to Hopf bifurcation points as (H1), (H2), etc., where (H1) is the first Hopf point to be reached if one traces the steady-state curve, starting at the the non-flaming steady-state corresponding to zero non-dimensionalized irradiance, the point (0,1) on our steady-state diagrams. Similarly we denote limit points as (L1), (L2), etc. The limit point (L1) is referred to as the 'ignition limit point'. The notation (CF) refers to a cyclic-fold bifurcation and (HCB) to a homoclinic bifurcation.

We use the notation $q_{\mathrm{ign}} \mid$ (L1) to denote the value of the non-dimensionalized irradiance ($q_{\mathrm{ign}}$) at which the limit point (L1) exists.

## 4. Results

When the gas-phase emissivity is 0.1 the steady-state structure of the model has been investigated in detail (Nelson 1998; M. I. Nelson 1998, unpublished work). In § 4 *a* we review those features of this work that are of particular interest from the perspective of polymer flammability: the existence of steady-state diagrams containing no limit points, the distinction between physically disjoint and non-physically disjoint steady-state diagrams, and the existence of 'smouldering combustion' states.

Using the characteristic temperature as the control parameter we show in which region of parameter space these structures are found.

In § 4 *b* we investigate the sensitivity of these results to variations in the emissivity of the gas phase, establishing in particular the change in the respective regimes of parameter space.

### (*a*) *Steady-state diagrams when* $\epsilon_{\mathrm{g}} = 0.1$

Figure 2*a* shows the steady-state diagram corresponding to the range $580 \leqslant T_{\mathrm{c}}\ (\mathrm{K}) \leqslant 676$; we label this structure type 1. The features of this diagram are a

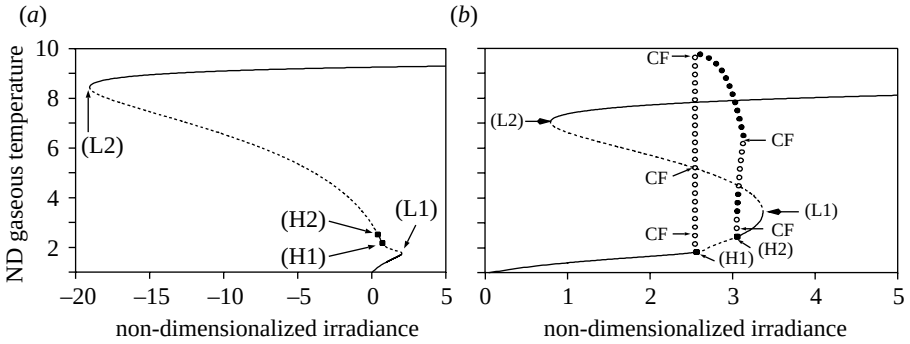


Figure 2. Representative type 1 ($580 \leqslant T_c\,(\mathrm{K}) \leqslant 676$) and type 6 ($794 \leqslant T_c\,(\mathrm{K}) \leqslant 845$) steady-state diagrams. Note that the steady states are physically disjoint in (*a*) and non-physically disjoint in (*b*). In (*b*) (H1) and (H2) are subcritical and supercritical Hopf points, respectively; the region of stability for the latter is too narrow to be identified on the figure. Parameter values: gas-phase emissivity, $\epsilon_g = 0.1$. The symbols and line types are defined in § 3 *a*. See also figure 3 for two additional steady-state diagrams using these parameter values, and figure 4, for the limit point bifurcation diagram for these parameter values. Part (*a*) reprinted from Nelson (1998). Parameter values: (*a*) $T_c = 620$ (K), (*b*) $T_c = 810$ (K).

low-valued stable steady-state branch, corresponding to a non-ignition event, a high valued stable steady-state branch, corresponding to the existence of a stable steady flame over the sample, a limit point in the right half-plane ($q_{\mathrm{ign}} \mid (\mathrm{L1}) > 0$), an ignition point, a limit point in the left half-plane $q_{\mathrm{ign}} \mid (\mathrm{L2}) < 0$, an extinction point, and two Hopf bifurcations. Depending upon the value of the characteristic temperature the (H2) point may be in either the right or the left half-plane. As the irradiance increases past $q_{\mathrm{ign}} \mid (\mathrm{L1})$ the only steady-state corresponds to a steady-flame over the surface of the material.

In type 1 steady-state diagrams, figure 2*a*, the periodic orbits generated by the Hopf bifurcation points (H1) and (H2) are unstable and when $q_{\mathrm{ign}} > q_{\mathrm{ign}} \mid (\mathrm{L1})$ the only stable attractor is the ignition branch. Consequently, although the transient addition of a gas-phase active fire retardant may perturb the system off the ignition branch, its long-term behaviour, after the additive has been consumed, is to return to the ignition branch.

Since only the right half-plane ($q_{\mathrm{ign}} \geqslant 0$) is physically meaningful, this steady-state diagram is physically disjoint, by which it is meant that the steady-state branches are not connected in the right half-plane—a distinction is drawn here between physically disjoint solution branches caused by the solution branch crossing the '$x = 0$' axis and the separate branches of solution that can arise from a well-defined bifurcation (Gray *et al*. 1991). Physically disjoint steady-state diagrams of the type shown in figure 2*a* are referred to as '0-disjoint' in the chemical engineering literature (Russo & Bequette 1995).

An important practical consequence of the physically disjoint structure is that it is not possible to extinguish the flame of such a material by decreasing the external irradiance sufficiently slowly. Furthermore, the flame is not guaranteed to self-extinguish if the irradiance is turned off instantaneously—when the irradiance is zero there are two stable attractors; a no-ignition state at ambient conditions and a state corresponding to a stable steady flame.

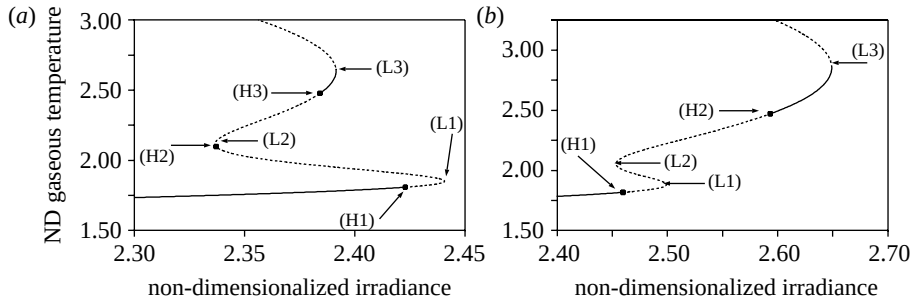


Figure 3. Representative steady-state diagrams for type 4 ($754 \leqslant T_c$ (K) $\leqslant 770$) and type 5 ($771 \leqslant T_c$ (K) $\leqslant 793$) structures. In both cases the steady-state diagrams are physically disjoint and the upper steady-state branch, corresponding to full combustion, is not shown. The transition from type 4 to type 5 is marked by the destruction of the Hopf bifurcation point (H2) by a co-dimension two bifurcation at the limit point (L2). Parameter values: gas-phase emissivity, $\epsilon_g = 0.1$; characteristic temperature, (*a*) $T_c = 765$ (K), (*b*) $T_c = 780$ (K). The symbols and line types are defined in § 3 *a*. See also figure 2, for two additional steady-state diagrams using these parameter values, and figure 4 for the limit point bifurcation diagram for these parameter values. Figure reprinted from Nelson (1998).

In our model the value of the non-dimensionalized variables on the ignition branch varies only weakly with the non-dimensionalized irradiance; we believe that for materials exhibiting physically disjoint steady-state diagrams the flame cannot be extinguished by lowering the irradiance to any physically attainable level, i.e. combustion is self-sustaining if the irradiance source is removed.

Although figure 2*b* contains two Hopf points and two limit points, the ordering of these bifurcations differs from that of figure 2*a* and the resulting steady-state diagram differs from it in respects that are important from the viewpoint of flammability. Here we concentrate on the most important difference: the (L2) limit point is now in the right half-plane and the steady-state digram is no longer physically disjoint. A material giving rise to such a steady-state diagram can no longer sustain a flame in the absence of an external irradiance; if the irradiance is reduced past a critical value, $q_{ign} \mid (L2)$, the flame will be extinguished.

A second phenomenon of practical interest is the existence of parameter regimes that have three stable steady-state branches, figure 3: a low-valued stable steady-state branch, corresponding to a non-ignition event; a high-valued stable steady-state branch, corresponding to the existence of a stable steady flame over the sample, not shown in figure 3; and, an intermediate branch. We refer to such steady-state diagrams as representing 'smouldering combustion' states.

Initially, the intermediate steady-state branch exists solely above the no-ignition branch (figure 3*a*, $q_{ign} \mid (L3) < q_{ign} \mid (L1)$). For higher values of the characteristic temperature we have $q_{ign} \mid (L3) > q_{ign} \mid (L1)$ and there are values of the irradiance for which only the intermediate branch and the combustion branch coexist (figure 3*b*).

Both of these situations offer the possibility of improved flammability characteristics, relative to figure 2*a*, as existence of the intermediate branch offers the prospect of permanently destabilizing the system, by a suitable perturbation, off the flame branch and onto a less 'dangerous' attractor. However, in the former the possibility of destabilizing the system onto the no-ignition branch already exists, so the intermediate state has not added a new mechanism for fire retardancy. In the latter case the

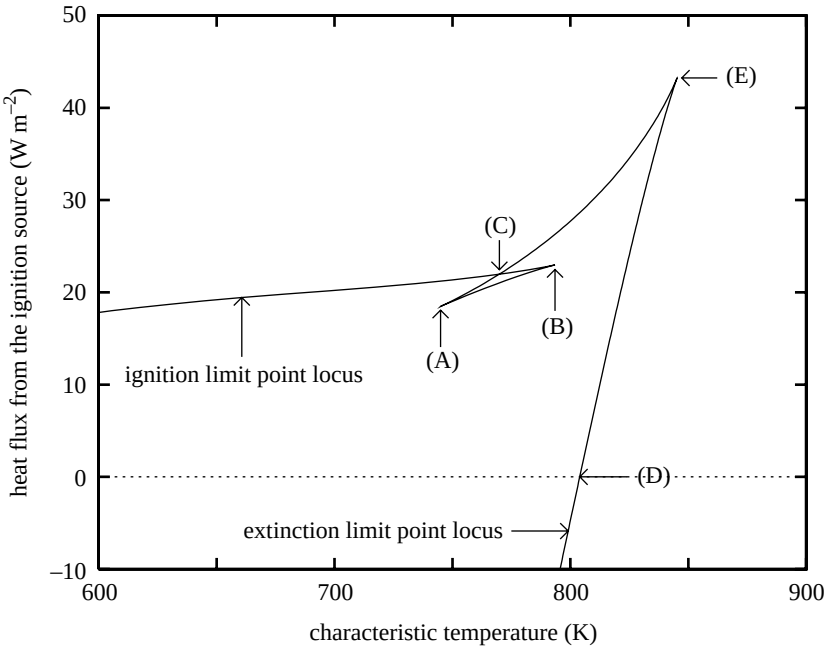


Figure 4. Limit point bifurcation diagram for a non-luminous flame (gas-phase emissivity, $\epsilon_g = 0.1$). The region between the cusp points (A) ($T_c \sim 744.9$ K) and (B) ($T_c \sim 793.5$ K) corresponds to the region in parameter space where 'smouldering combustion' states exist. Point (C) ($T_c \sim 769.9$ K) is the double limit point bifurcation, the region between (C) and (B) is of greater practical interest than that between (A) and (C). Point (D) ($T_c \sim 804$ K) marks the transition from physically disjoint to non-physically disjoint steady-state diagrams. The cusp point (E) ($T_c \sim 845.3$ K) marks the final destruction of the limit point locus. The dependence of the points (A)–(E) with gas-phase emissivity is shown in figure 5. Examples of steady-state diagrams corresponding to four slices from this diagram are shown in figures 2–3. Other examples of limit point bifurcation diagrams are shown in figures 6 (luminous flame) and 7 (non-luminous flames).

intermediate branch does not coexist with the no-ignition branch; in the absence of the intermediate branch any small perturbation would eventually lead to the system restabilizing itself on the flame steady state, so that the existence of the intermediate steady state improves the prospects for fire retardancy.

In moving from figure 3*a* to figure 3*b* there must be a characteristic temperature for which the value of the non-dimensionalized irradiance at which the limit points (L1) and (L3) occur is the same ($q_{ign} \mid (L3) = q_{ign} \mid (L1)$); such a point is called a double-limit point (Gray & Roberts 1988). In view of the discussion in the preceding paragraph, materials 'above' the double limit point are of greater interest than those 'below' it.

Although the relative positions of the Hopf and limit points determine the mechanism by which a material ignites, it is the steady-state curves, rather than the structure of the periodic orbits, that is of most importance when considering flammability and fire retardancy (Nelson 1998). The features of interest are readily determined from the limit point bifurcation curve (figure 4). From this figure the characteristic temperature range corresponding to the existence of smouldering combustion states,

the value at which the physically disjoint steady-state structure is destroyed, and the cusp point corresponding to the final limit point annihilation can be determined.

It is clearly desirable for a material to possess neither limit points nor Hopf bifurcations on its steady-state diagram. Such materials cannot exhibit large changes in steady-state temperature to small changes in the imposed irradiance and are characterized as being 'intrinsically non-flammable'. This is investigated elsewhere (M. I. Nelson 1998, unpublished work).

### (*b*) *The influence of gas-phase emissivity ($\epsilon_g$) upon flammability*

In § 4 *a* we reviewed some of the steady-state structures that exist for non-luminous flames ($\epsilon_g = 0.1$; figures 2 and 3), and illustrated how they could be identified from the limit point bifurcation diagram (figure 4). In this section we investigate how the features of interest on the limit point bifurcation diagram change as the emissivity of the flame varies (figure 5). In § 4 *b* (i) we consider the range $0.07 \leqslant \epsilon_g \leqslant 1$, while in § 4 *b* (ii) we consider the range $0 \leqslant \epsilon_g \leqslant 0.07$.

Many materials burn with a 'sooty flame' and therefore the region $0.07 \leqslant \epsilon_g \leqslant 1$ is of greatest interest. Formally, our model only applies to materials undergoing a single-step decomposition leaving behind no solid residue, equation (2.1), such as polymethylmethacrylate. Under some circumstance our model applies to the combustion of carbonaceous chars. Consider a material forming a carbonaceous char, which has the following pyrolysis reaction scheme:

$$\mathcal{M}_1(\mathrm{s}) \rightarrow \mathcal{M}_2(\mathrm{g}) + \mathcal{M}_c(\mathrm{s}), \tag{4.1}$$

$$\mathcal{M}_c(\mathrm{s}) \rightarrow \mathcal{M}_4(\mathrm{g}), \tag{4.2}$$

where $\mathcal{M}_c(\mathrm{s})$ represents the char. Provided that pyrolysis of the original material (equation (4.1)) occurs over a quite distinct temperature range to that of pyrolysis of the char (equation (4.2)) we can regard the combustion of such a material as effectively two separate processes, with our model applying to the second. Carbonaceous char often burns with a flame of low luminosity and hence emissivity, i.e. the region $0 \leqslant \epsilon_g \leqslant 0.07$.

#### (i) *The region* $0.07 \leqslant \epsilon_g \leqslant 1$

For a fixed value of the emissivity, crossing line (D) in figure 5 marks the transition from physically disjoint to non-physically disjoint steady-state structures. Similarly, crossing line (E) represents the transition from a steady-state diagram with limit points to a steady-state diagram with no limit points. As the emissivity increases the characteristic temperature at which these transitions occurs increases. This increase is undesirable because the higher the characteristic temperature at these transitions the less likely it is that a material will exhibit either non-physically disjoint steady-state structures or a steady-state diagram with no limit points.

For a fixed value of the emissivity the interval between the lines (A) and (B) is the region in which 'smouldering combustion' states exist; line (A) marks the formation of such states, while line (B) marks their destruction. Line (C) is the double limit point locus. As discussed in § 4 *a*, it is the interval between the lines (B) and (C) that is of greater importance.

Line (A) shows little variation as the emissivity increases. However, lines (B) and (C) decrease with increasing emissivity and when $\epsilon_g \sim 0.3$ all three merge at a quartic

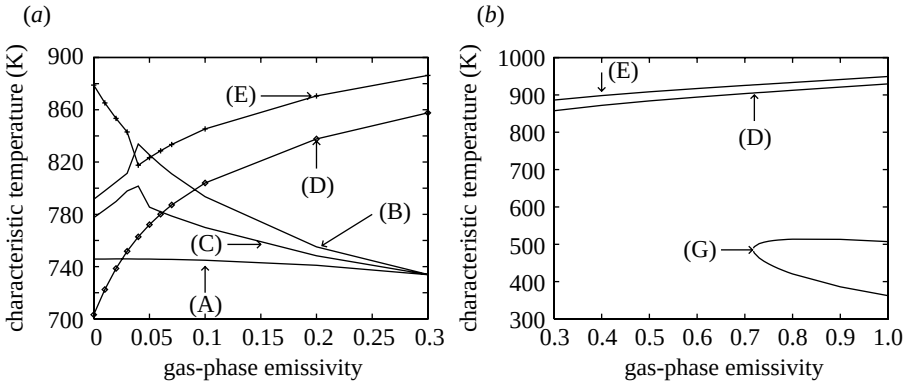


Figure 5. The dependence of flammability regimes upon the flame emissivity. For a fixed value of the emissivity the points (A)–(E) are defined in figure 4, and the region (G) is defined in figure 6. The point of intersection of lines (A), (B) and (C) is a quartic fold bifurcation (Gray & Roberts 1988). Examples of limit point bifurcation diagrams corresponding to four slices from this diagram are shown in figures 4, 6 and 7.

fold bifurcation (Gray & Roberts 1988); for sufficiently large flame emissivities there are no 'smouldering combustion' states.

The locus (G) in figure 5*b* delimits a region wherein the ignition limit point does not increase monotonically with characteristic temperature. Figure 6*a* shows the limit point locus for the case $\epsilon_{\mathrm{g}} = 0.8$. As indicated in figure 5*b* this system has no more than two limit points; there are no values of the characteristic temperature for which 'smouldering combustion' states exist. The boxed region is expanded in figure 6*b*, showing that over the region $420.6 \leqslant T_{\mathrm{c}}\,(\mathrm{K}) \leqslant 513.7$ the ignition limit point *decreases* with increasing characteristic temperature: this feature is surprising.

To summarize the results of this section, in the region $0.07 \leqslant \epsilon_{\mathrm{g}} \leqslant 1$ increasing emissivity corresponds to decreasing fire-retardant properties.

(ii) *The region* $0 \leqslant \epsilon_{\mathrm{g}} \leqslant 0.07$

The flame emissivities in this section represent materials burning with low luminosity flames and are of less practical interest than those in § 4 *b* (i). Accordingly the only feature of figure 5*a* we discuss is the apparent crossing-over of the lines (B) and (E). At first sight this suggests that there are values of the characteristic temperature and flame emissivity for which the cusp point ending the region of 'smouldering combustion' states, line (B), occurs after the cusp point destroying all remaining limit points, line (E).

In figure 7 we show two limit point bifurcation diagrams for low emissivity materials; in figure 7*a* the cusp points delimiting the region of 'smouldering combustion' states occur on the extinction limit point locus, in contrast to figure 4 where they occur on the ignition limit point locus. As the emissivity is increased from zero, these cusp points move 'up' the extinction limit point locus, towards the cusp point (E), which marks the 'final destruction' of limit points in the system. However, when the emissivity is in the range $\epsilon_{\mathrm{g}} \sim 0.04 - 0.05$, the cusp point marking the destruction of the 'smouldering combustion' states extends past the limit point (E) (figure 7*b*). This means that the smouldering combustion states are now formally destroyed at

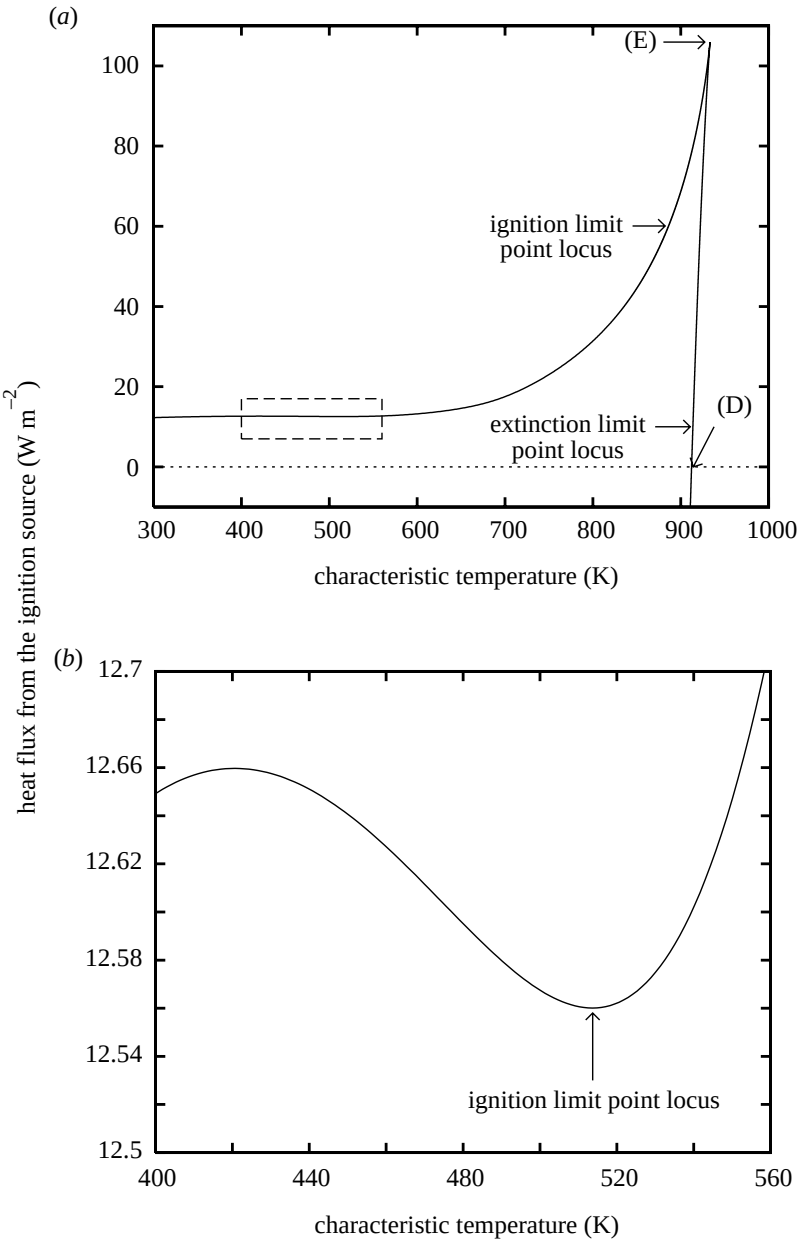


Figure 6. Limit point bifurcation diagram for a luminous flame (gas-phase emissivity, $\epsilon_g = 0.8$). Point (D) ($T_c \sim 912.3$ K) marks the transition from physically disjoint to non-physically disjoint steady-state diagrams. The cusp point (E) ($T_c \sim 933.5$ K) marks the final destruction of the limit point locus. When the characteristic temperature is in the range $420.6 \leqslant T_c$ (K) $\leqslant 513.7$, the non-monotonicity region, the ignition limit point *decreases* with increasing characteristic temperature. The dependence of the points (D) and (E) with gas-phase emissivity is shown in figure 5. Other examples of limit point bifurcation diagrams are shown in figures 4 and 7, both non-luminous flames.

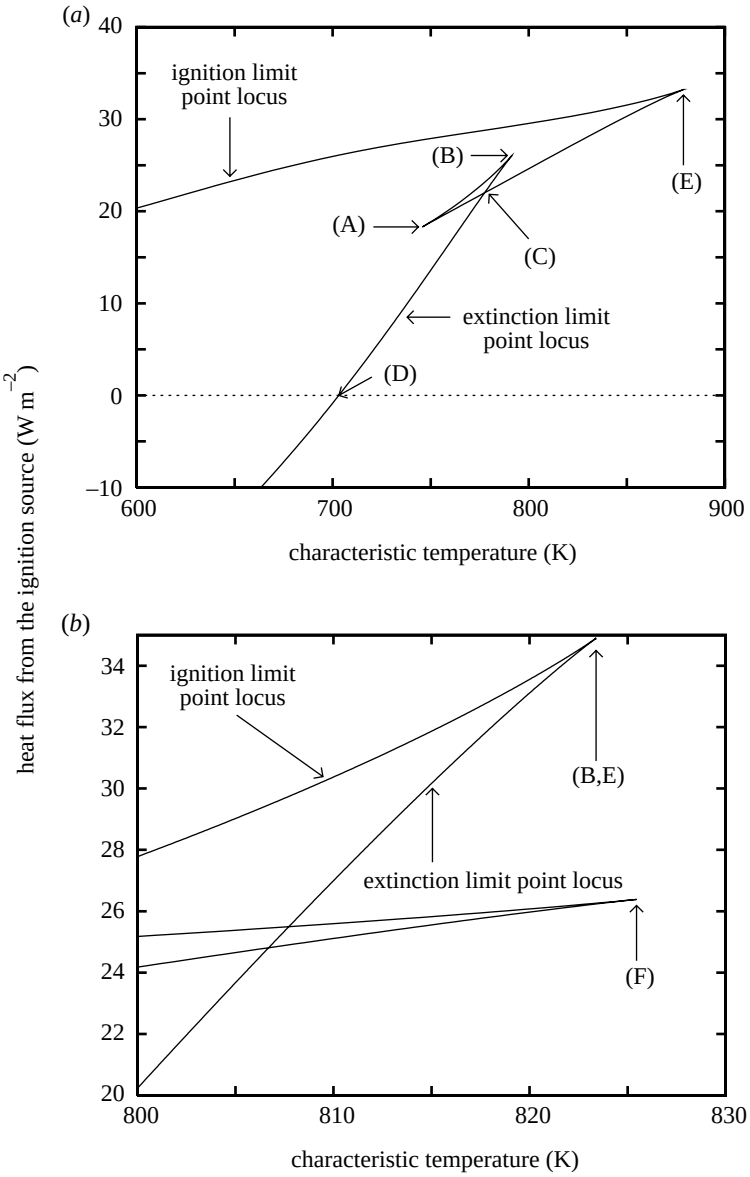


Figure 7. Limit point bifurcation diagrams for non-luminous flames. The region between the cusp points (A) ($T_c \sim 745.8$ K in ($a$) and (B) ($T_c \sim 791.5$ K in ($a$), $T_c \sim 823.4$ K in ($b$) corresponds to the region in parameter space where 'smouldering combustion' states exist. Point (C) ($T_c \sim 777.4$ K in ($a$) is the double limit point bifurcation, the region between (B) and (C) is of greater practical interest than that between (A) and (B). Point (D) ($T_c \sim 703.2$ K in ($a$) marks the transition from physically disjoint to non-physically disjoint steady-state diagrams. The cusp points (E) in ($a$), $T_c \sim 878.9$ K, and (F) in ($b$), $T_c \sim 825.5$ K mark the final destruction of the limit point locus. The dependence of the points (A)–(E) with gas-phase emissivity is shown in figure 5. Other examples of limit point bifurcation diagrams are shown in figures 4 (non-luminous flame) and 6 (luminous flame). Parameter values: ($a$) $\epsilon_g = 0$, ($b$) $\epsilon_g = 0.05$.

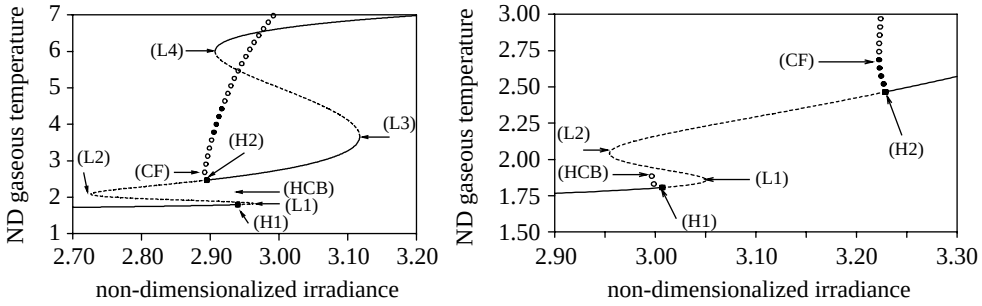


Figure 8. Representative type 5 and type 6b steady-state diagrams for the situation when the 'smouldering combustion' states are on the extinction limit point branch, figure 7. The transition from type 5 to type 6b is the self-annihilation of the (L2) and (L3) limit points. Compare with figure 2*b* and figure 3*b* for the situation when the 'smouldering combustion' states are on the ignition limit point branch, figure 4. In both (*a*) and (*b*) (H1) and (H2) are subcritical and supercritical Hopf bifurcations respectively. In (*a*) the maximal non-dimensionalized gaseous temperature of the orbits generated by (H1) are too small to appear on the figure, these orbits are unstable. Additionally, the region of stability of (H2) is too narrow to be identified (*a*). Parameter values: gas-phase emissivity, $\epsilon_{\mathrm{g}} = 0.03$; characteristic temperature, (*a*) $T_{\mathrm{c}} = 800$ (K), (*b*) $T_{\mathrm{c}} = 820$ (K).

the cusp point (E) and that the final limit points are destroyed at the cusp point (F) in figure 7*b*; the meaning attached to the cusp points is reversed.

Materials with $0 \leqslant \epsilon_{\mathrm{g}} \leqslant 0.07$, when the 'smouldering combustion' cusp points are on the extinction limit point locus, show the same progression of steady-state diagrams, type 1 to type 5, as materials where the 'smouldering combustion' cusp points are on the ignition limit point locus. However, the steady-state diagrams formed following the destruction of the type 5 steady-state diagrams differ in these two cases, although in both the demise of the type 5 structure is marked by the collision of two limit points: for the latter the (L1) and (L2) limit points collide, see figures 2*b* and 3*b*, while for the former it is the (L3) and (L4) that collide (figure 8).

## 5. Discussion

The design of fire-retarded materials exploits two approaches: the synthesis of new materials that have a lower flammability than existing materials, and the fire retardancy of existing materials by the addition of suitable additives. In practice these two mechanisms are often interlinked.

We can describe in mathematical terms what properties are desirable to reduce flammability:

1. ideally, an absence of limit point bifurcations in the steady-state diagrams;

2. where limit points do exist, materials exhibiting non-physically disjoint steady-state diagrams have enhanced fire-resistant properties over those that do not;

3. if neither of the two options above is available, look for 'smouldering combustion' states.

In this paper we have investigated the way in which such properties depend upon the characteristic temperature of the pyrolysis reaction and the emissivity of the flame. This can be considered as a search to define the properties required by fire-retarded combustible materials.

For a fixed value of the emissivity it is always theoretically possible to find a material that either has a non-physically disjoint bifurcation diagram or has no limit points. However, as the emissivity increases, it becomes increasingly difficult to achieve this; the characteristic temperature at which these transitions occurs increases (figure 5). Furthermore, as the emissivity increases, the range of characteristic temperature over which 'smouldering combustion' states are exhibited decreases; for sufficiently high emissivity such states do not exist (figure 5). Hence increasing emissivity decreases the possibility of smouldering combustion and increases the flammability.

How can one increase the fire retardancy of a material with a specific emissivity and characteristic temperature? The ideal solution is to introduce an additive that brings either of the two more desirable transition temperatures below the material's characteristic temperature. Failing that, the additive may promote 'smouldering combustion' states. The last is not an ideal solution because a smouldering material constitutes a source for further ignition in a real fire.

Mathematically, one can envisage a systematic investigation of the model parameters, to find out to which parameter these transition temperatures are most sensitive. This would lead to suggestions as to what types of additive would be most effective at retarding a given material. Figure 5 strongly suggests that it is more difficult to retard materials with high emissivity flames.

Figure 6 reveals the surprising fact that for sufficiently high emissivity the ignition limit point is not monotone with characteristic temperature. In fire-engineering terminology the ignition limit point locus corresponds to the critical heat flux, the smallest heat flux that will ignite a material under ambient conditions. In thermal pyrolysis models (Drysdale 1987) and critical heat flux models (Nelson *et al*. 1995) the critical heat flux is monotone increasing with increasing characteristic temperature. These results are not surprising; the characteristic temperature is a crude estimate of the temperature at which a material decomposes, and increasing characteristic temperature corresponds to increased thermal stability. One would therefore expect that increasing the characteristic temperature corresponds to decreased flammability.

The non-monotonicity is a consequence of the subtle nonlinear coupling in this model. While increasing the emissivity increased the rate of energy loss from the flame, decreasing the flame temperature, it increases the rate of energy transfer from the flame to the solid. Evidently, there is competition between the decrease in flame temperature, due to increase heat loss by radiation, and increase in heat-transfer to the solid, by increased emissivity. However, it is not possible experimentally to distinguish the change in critical heat flux shown in figure 6*b*.

Although we have emphasized the importance of materials that cannot undergo self-sustaining combustion, it is not possible to distinguish between materials that exhibit self-sustaining and non self-sustaining combustion in the cone calorimeter. The cone calorimeter test method specifies that the irradiance is held constant throughout the test. Furthermore, the radiating elements cool down very slowly, so even if their power source is turned off instantaneously, the irradiance experienced

by the sample decreases only slowly; there is a strong likelihood that the sample will fully burn before the irradiance has decreased to zero. So although the cone calorimeter is an important tool for investigating flammability, it should not be regarded as the only tool that is required.

## 6. Summary

Using a dynamical systems model for the ignition of polymeric materials we have outlined how desirable flame-retardant features can be identified from the limit point bifurcation diagram. Of particular importance is the possibility of eliminating all limit points and, failing that, the construction of non-physically disjoint steady-state diagrams. Of lesser importance is the possibility of materials exhibiting 'smouldering combustion' states.

We have found that as the emissivity of the flame increases, the region of parameter space in which materials have such desirable properties decreases, and, in the case of 'smouldering combustion' states, may disappear altogether. The techniques used in this paper can be used to identify the types of fire retardants that will be most effective at decreasing the flammability of a given material.

Finally, although the cone calorimeter is an important tool for investigating the flammability of polymeric materials, it is important to realize that its current mode of operation imposes some restrictions on the questions that it can answer.

This work was carried out while M.I.N. was supported by a fellowship from the Royal Society to work in the Division of Science and Technology at the University of Auckland (New Zealand).

## Appendix A. Nomenclature

The subscript 's' refers to a property of the solid phase, subscript 'g' to a property of the gas phase, the subscript 0 to the solid–volatile boundary and subscript 1 to the volatile–ambient boundary. The subscript $i$ is used when a parameter may take either the subscript g or s.

| | | |
|---|---|---|
| $A_i$ | Pre-exponential factor | ($s^{-1}$) |
| $E_i$ | Activation energy | (J $mol^{-1}$) |
| $\mathcal{F}$ | Integrated configuration factor between the solid and the gaseous reaction zone | (—) |
| $\mathcal{F}_{gs}$ and $\mathcal{F}_{sg}$ | Integrated configuration factors $\mathcal{F}_{gs} = \mathcal{F}_{sg} = \mathcal{F}$ | (—) |
| $\mathcal{H}$ | Ramping rate used in the thermogravimetric experiment | (K $s^{-1}$) |
| $\mathcal{L}$ | Heat flux from the ignition source per unit area of the solid surface | (W $m^{-2}$) |
| $\mathcal{M}_1$ | Mass of the test material | (kg) |
| $\mathcal{M}_2$ | Mass of the gaseous fuel | (kg) |
| $\mathcal{M}_3$ | Mass of the gaseous product | (kg) |
| $\mathcal{M}_i(0)$ | The mass of species $i$ at time $t = 0$ | (kg) |
| $\mathcal{P}^0$ | Standard atmospheric pressure | (N $m^{-2}$) |
| $Q_i$ | Heat of reaction | (J $kg^{-1}$) |

| | | |
|---|---|---|
| $R$ | Ideal gas constant | ($\mathrm{J\,K^{-1}\,mol^{-1}}$) |
| $R_p$ | Mass flow of fuel into the gaseous reaction zone | ($\mathrm{kg\,s^{-1}}$) |
| $S$ | Surface area of the test material | ($\mathrm{m^2}$) |
| $T_i$ | Temperature | (K) |
| $T_i(0)$ | The temperature at time $t = 0$ | (K) |
| $T_i^*$ | Non-dimensionalized temperature $T_i^* = T_i/T_\mathrm{a}$ ($i = \mathrm{g}$, $i = \mathrm{s}$) | (—) |
| $T_\mathrm{a}$ | Ambient temperature | (K) |
| $T_\mathrm{c}$ | Characteristic temperature of the pyrolysis reaction | (K) |
| $V_i$ | Volume | ($\mathrm{m^3}$) |
| $V_p$ | Volume per kilogram of $\mathcal{M}_2$ (calculated using the ideal gas law) | ($\mathrm{m^3\,kg^{-1}}$) |
| $\mathcal{W}_2$ | Molecular weight of species $\mathcal{M}_2$ | ($\mathrm{kg\,mol^{-1}}$) |
| $\mathcal{W}_3$ | Molecular weight of species $\mathcal{M}_3$ | ($\mathrm{kg\,mol^{-1}}$) |
| $Z_i$ | Non-dimensionalized activation energy, $Z_i = E_i/(RT_\mathrm{a})$ | (—) |
| $b_k$ | The number of kilograms of oxygen that are consumed in the complete combustion of 1 kg of $\mathcal{M}_2$ | |
| $c_{p_i}$ | Specific heat capacity | ($\mathrm{J\,K^{-1}\,kg^{-1}}$) |
| $k$ | First-order reaction rate | ($\mathrm{kg\,s^{-1}}$) |
| $q_\mathrm{ign}$ | Non-dimensionalized heat-flux from the ignition source ($q_\mathrm{ign} = \mathcal{L}/(T_\mathrm{a}\chi_0)$) | (—) |
| $q_\mathrm{ign} \mid (\mathrm{Li})$ | The value of the non-dimensionalized irradiance at which the limit point Li exists | (—) |
| $q_\mathrm{inflow}$ | Volumetric flow rate caused by decomposition of the test material | ($\mathrm{m^3\,s^{-1}}$) |
| $q_\mathrm{reaction}$ | Volumetric flow rate produced by the gaseous reaction | ($\mathrm{m^3\,s^{-1}}$) |
| $t$ | Time | (s) |
| $x$ | Width of the test material | (m) |
| $y$ | Length of the test material | (m) |
| $\alpha_i$ | Absorptivity, $\alpha_i = \epsilon_i$ | (—) |
| $\delta_i$ | Thickness | (m) |
| $\chi_0$ | Heat transfer coefficient between the solid sample and the gaseous reaction zone | ($\mathrm{W\,m^{-2}\,K^{-1}}$) |
| $\chi_1$ | Heat transfer coefficient between the gaseous reaction zone and the surrounding air | ($\mathrm{W\,m^{-2}\,K^{-1}}$) |
| $\epsilon_i$ | Emissivity, $\epsilon_i = \alpha_i$ | (—) |
| $\rho_i$ | Density | ($\mathrm{kg\,m^{-3}}$) |
| $\sigma$ | Stefan–Boltzmann constant | ($\mathrm{W\,m^{-2}\,K^{-4}}$) |

Unless otherwise specified we take the following typical parameter values:

$$A_{\mathrm{g}} = 10^{12}\ (\mathrm{s}^{-1}), \qquad E_{\mathrm{g}} = 150\ (\mathrm{kJ\ mol}^{-1}),$$
$$E_{\mathrm{s}} = 80\ (\mathrm{kJ\ mol}^{-1}), \qquad \mathcal{F}_{\mathrm{gs}} = \mathcal{F}_{\mathrm{sg}} = 1,$$
$$\mathcal{H} = 1/60\ (\mathrm{K\ s}^{-1}), \qquad Q_{\mathrm{g}} = 30\,000\ (\mathrm{kJ\ kg}^{-1}),$$
$$Q_{\mathrm{s}} = -1000\ (\mathrm{kJ\ kg}^{-1}), \qquad S_0 = 0.0625\ (\mathrm{m}^2),$$
$$T_{\mathrm{a}} = 298\ (\mathrm{K}), \qquad T_{\mathrm{c}} = 620\ (\mathrm{K}),$$
$$\mathcal{W}_2 = 0.1\ (\mathrm{kg\ m}^{-3}), \qquad \mathcal{W}_3 = 0.02\ (\mathrm{kg\ m}^{-3}),$$
$$c_{p_{\mathrm{g}}}\rho_{\mathrm{g}} = 1.04 \times 10^3\ (\mathrm{J\ K}^{-1}\ \mathrm{m}^{-3}), \qquad c_{p_{\mathrm{s}}} = 1\ (\mathrm{kW\ m}^{-2}\ \mathrm{K}^{-1}),$$
$$x = y = 0.25\ (\mathrm{m}), \qquad \chi_0 = \chi_1 = 30\ (\mathrm{W\ m}^{-2}\ \mathrm{K}^{-1}),$$
$$\delta_{\mathrm{s}} = 0.001\ (\mathrm{m}), \qquad \delta_{\mathrm{g}} = 0.016\ (\mathrm{m}),$$
$$\epsilon_{\mathrm{s}} = \alpha_{\mathrm{s}} = 1, \qquad \rho_{\mathrm{s}} = 2000\ (\mathrm{kg\ m}^{-3}),$$
$$V_{\mathrm{g}} = 10^{-3}\ (\mathrm{m}^3).$$

The value of the gas-phase emissivity, $\epsilon_{\mathrm{g}}$, is assumed to lie in the range $0 \leqslant \epsilon_{\mathrm{g}} \leqslant 1$.

For simplicity, gas and solid phase properties are greatly idealized. Thus thermophysical properties of the gas and solid phases are assumed to be temperature independent.

The appropriate values for the physical constants are $\mathcal{P}^0 = 101\,325\ (\mathrm{N\ m}^{-2})$, $R = 8.314\,41\ (\mathrm{J\ K}^{-1}\ \mathrm{mol}^{-1})$, and $\sigma = 5.67 \times 10^{-8}\ (\mathrm{J\ s}^{-1}\ \mathrm{m}^{-2}\ \mathrm{K}^{-4})$.

## References


Babrauskas, V. 1984 Development of the cone calorimeter—a bench scale heat release rate apparatus based on oxygen consumption. *Fire Mater.* **8**, 81–95.

Babrauskas, V. & Parker, W. J. 1986 Ignitability measurements with the cone calorimeter. NBSIR 86-3445. Gathersburg, MD: National Bureau of Standards.

Búcsi, A. & Rychlý, J. 1992 A theoretical approach to understanding the connection between ignitability and the flammability parameters of organic polymers. *Polym. Degrad. Stability* **38**, 33–40.

Doedel, E. & Kernevez, J. P. 1986 AUTO: software for continuation and bifurcational problems in ordinary differential equations. Applied Mathematics Report, California Institute of Technology, Pasadena, CA 91125.

Doedel, E., Wang, X. & Fairgrieve, T. 1994 AUTO94: software for continuation and bifurcation problems in ordinary differential equations. Applied Mathematics Report, California Institute of Technology, Pasadena, CA 91125.

Drysdale, D. 1987 *An introduction to fire dynamics*, 1st edn. Wiley.

Gray, B. F. & Roberts, M. J. 1988 A method for the complete qualitative analysis of two coupled ordinary differential equations dependent on three parameters. *Proc. R. Soc. Lond.* A **416**, 361–389.

Gray, B. F., Merkin, J. H. & Wake, G. C. 1991 Disjoint bifurcation diagrams in combustion systems. *Math. Comput. Modelling* **15**, 25–33.

Hatakeyama, T. & Quinn, F. X. 1994 *Thermal analysis: fundamentals and applications to polymer science*, 1st edn. Wiley.

Nelson, M. I. 1998 Ignition mechanisms of thermally thin thermoplastics in the cone calorimeter. *Proc. R. Soc. Lond.* A **454**, 789–814.

Nelson, M. I., Brindley, J. & McIntosh, A. C. 1995 The dependence of critical heat flux on fuel and additive properties: a critical mass flux model. *Fire Safety J.* **24**, 107–130.

Nelson, M. I., Brindley, J. & McIntosh, A. C. 1996*a* Ignition properties of thermally thin materials in the cone calorimeter: a critical mass flux model. *Combust. Sci. Technol.* **113–114**, 221–241.

Nelson, M. I., Brindley, J. & McIntosh, A. C. 1996*b* Ignition properties of thermally thin thermoplastics—the effectiveness of inert additives in reducing flammability. *Polym. Degrad. Stability* **54**, 255–267.

Nelson, M. I., Brindley, J. & McIntosh, A. C. 1997 The effect of heat sink additives on the ignition and heat release properties of thermally thin thermoplastics. *Fire Safety J.* **28**, 67–94.

Russo, L. P. & Bequette, B. W. 1995 Impact of process design on the multiplicity behaviour of a jacketed exothermic CSTR. *AIChE J.* **41**, 135–147.

Rychlý, J. & Costa, L. 1995 Modelling of polymer ignition and burning adopted for cone calorimeter measurements: the correlation between the rate of heat release and oxygen index. *Fire Mater.* **19**, 215–220.

Rychlý, J. & Rychlá, L. 1986 Effect of flame retardants on polyolefines. *Fire Mater.* **10**, 7–10.

Rychlý, J. & Rychlá, L. 1996 Modelling of heat-release rate-time curves from cone calorimeter for burning of polymers with intumescence additives. *Polym. Degrad. Stability* **54**, 249–254.